JOURNAL OF AIRCRAFT
Vol. 45, No. 5, September–October 2008

Transition Measurement of Natural Laminar Flow Wing on Supersonic Experimental Airplane NEXST-1

Naoko Tokugawa,* Dong-Youn Kwak,† and Kenji Yoshida‡
Japan Aerospace Exploration Agency, Tokyo 181-0015, Japan
and
Yoshine Ueda§
Tokyo Business Service Company, Ltd., Tokyo 181-0015 Japan

DOI: 10.2514/1.33596

Flight testing of an unmanned and scaled supersonic experimental airplane NEXST-1 is performed by the Japan Aerospace Exploration Agency to validate computational-fluid-dynamics-based aerodynamic design technology. This is the first attempt to apply the natural laminar flow wing concept to a supersonic vehicle. The concept of the natural laminar flow wing is validated by measuring the surface pressure and the transition locations of the boundary layer. In this paper, the results of the transition measurement are introduced and compared with the numerically predicted results. The transition locations detected experimentally are in good agreement with the predicted locations, and the natural laminar flow effect is confirmed in the aerodynamic design conditions of the supersonic experimental airplane NEXST-1.

Nomenclature

C	=	local chord length
C_L	=	lift coefficient of full configuration
C_p	=	surface pressure coefficient
Cp_{rms}	=	fluctuation (rms) of surface static pressure of the wind tunnel
E	=	dc output of the hot-film sensor
e	=	ac output of the hot-film sensor
H	=	altitude
M	=	Mach number
p	=	local surface pressure measured by the dynamic pressure transducer
P_{PRT}	=	local total pressure measured by the Preston tube
Re_c	=	Reynolds number based on the mean aerodynamic chord
S	=	semispan length
T_{blow}	=	time from the beginning of the blow in the wind-tunnel test
T_{lo}	=	time from the liftoff in the flight test
T_{TC}	=	local temperature measured by the thermocouple
X	=	chordwise position
X_{tip}	=	axial length from the tip of the wind-tunnel model
Y	=	spanwise position
α	=	angle of attack
φ	=	circumferential angle from the top line on the nose
$'$	=	fluctuation

Received 20 July 2007; accepted for publication 16 October 2007.

*Associate Senior Researcher, Supersonic Transport Team, Aviation Program Group, 6-13-1 Osawa, Mitaka.
†Associate Senior Researcher, Supersonic Transport Team, Aviation Program Group, 6-13-1 Osawa, Mitaka. AIAA Member.
‡Manager for Planning, Program Office, Aviation Program Group, 7-44-1 Jindaiji-Higashimachi, Chofu. AIAA Member.
§Researcher, Supersonic Transport Team, 6-13-1 Osawa, Mitaka.

Introduction

DRAG reduction is one of the most important technical problems still to be addressed to make the next generation of supersonic transport flyable. Therefore, at the Japan Aerospace Exploration Agency (JAXA), the National Experimental Supersonic Transport (NEXST) program [1–3] has been underway to develop computational-fluid-dynamics-based aerodynamic design technology to design a low-drag configuration (Fig. 1). The main aim is to reduce friction drag under supersonic cruise conditions at $M = 2.0$ and $C_L = 0.10$.

Four aerodynamic design concepts are applied to realize the low drag of the configuration [4]. The warped wing [5] and the arrow planform wing [6] are applied to reduce the lift-dependent drag, and the area-ruled body [7] is adopted to reduce the wave drag due to volume. Then the natural laminar flow (NLF) concept is applied to the upper surface of the main wing, the main purpose being to reduce the friction drag [4,8,9]. This NLF concept is the most original design. The natural laminarization on the swept wing with a subsonic leading edge used to be believed unachievable at supersonic speed, because the crossflow instability will lead the early boundary-layer transition at the leading-edge region.

But in this project, the NLF concept is applied for the first time anywhere, based on the recent development of computational fluid dynamics (CFD) technology and the transition prediction method. The boundary-layer transition on the 3-D wing is generally known to be governed by the crossflow instability in the leading-edge region. And, in the following adverse pressure gradient region, the Tollmien-Schlichting (T-S) wave type instability will grow. But we expect that the NLF effect can be obtained, based on the following two ideas for pressure gradient: one is the minimization of the distance between the leading edge and suction peak to suppress growth of the crossflow instability, and the other is the negligible adverse pressure gradient after the suction peak to suppress the T-S wave-type instability. To obtain a wing section achieving the surface pressure distribution as a design target, we developed a CFD-based "inverse" design method [10]. The inverse design method is a method to obtain the wing section through iterating modification of the wing section to make its surface pressure distribution coincident with the target optimum pressure distribution. The transition location on the upper surface of the designed wing is predicted by the e^N method using a numerical code dubbed "LSTAB" and developed at JAXA, based on the linear stability theory in the 3-D compressible boundary layer [11–13]. The transition location predicted by LSTAB was expected to be a location far to the back, such as $45 \sim 60\%$ C at the design point with a lift

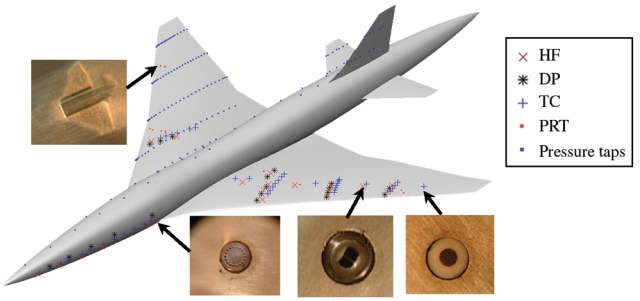

Fig. 1 Sensor position.

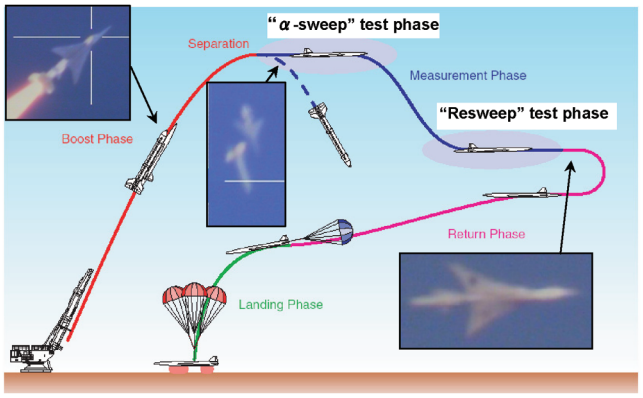

Fig. 2 Supersonic experimental airplane NEXST-1 and outline of the flight test.

coefficient of full configuration $C_L = 0.10$, though it moved forward considerably under these conditions except for the design point. Therefore, the NLF effect may be expected on the designed wing. The NLF effect on the wing designed by the inverse design method has been validated by means of wind-tunnel tests using wing–body configuration models [14,15]. However, the freestream disturbance in usual supersonic tunnels is relatively large and the unit Reynolds number is lower than in flight conditions. Thus, the aerodynamic design concept must be validated in flight. Therefore, JAXA conducted a flight test using an unmanned and scaled supersonic experimental airplane, in the first attempt to measure the boundary-layer transition in a supersonic flight test in Japan (Fig. 2).

The purpose of this paper is to introduce the transition measurement of this supersonic experimental airplane, which is called NEXST-1. First of all, the measurement system is introduced, along with examinations of its function through preliminary tests on the ground. Then, the results of the transition measurement obtained in the flight test are presented and compared with the numerical prediction.

Transition Measurement Systems

Outline

The four types of sensors used to detect the transition location in the NEXST-1 experimental airplane were hot-film sensor (HF), dynamic pressure transducer (DP), thermocouple (TC), and Preston tube (PRT) (Fig. 1) [16].

These sensors were mainly distributed in arrays of spanwise position with a normalized semispan length $Y/S \approx 0.3, 0.5, 0.7$ for the left wing (Fig. 1) and on the left side of the nose. The reason mainly the left side was used for transition measurements was that any turbulence in the right wing and right side of the nose areas was assumed to be caused by the pitot probe (air data sensor probe), which protrudes from the right side of the nose. These sensors were installed on the surface of the NEXST-1 airplane with a permitted step of less than 40 μm and were arranged at an inclination of $15 \sim 20$ deg on the wing side to the flow direction so that the upstream sensor did not disturb the downstream boundary layer (Fig. 1). The three kinds of sensors, other than the Preston tube, were arranged to supplement each other in a row. The Preston tube was positioned separately from the other three flush-mounted sensors, as it causes considerable surface roughness and disturbs the downstream boundary layer (Fig. 1). On the other hand, each sensor was shifted 10 or 15 deg in a circumferential direction on the nose. In general, inflow and outflow at the gap between the sensor and the body can disturb the boundary layer and promote transition. Therefore, the sealant was thickened around the sensor inside the body to prevent leaks. Moreover, it was confirmed that there were no leaks as pressure was absorbed at the gap between the sensor and the body.

Hot-Film Sensor and Dynamic Pressure Transducer

The hot film measures surface shear stress and its fluctuation. The sensor was equivalent to the DANTEC 55R45 (Fig. 1), but was a custom-made item in an L shape suitable to mount on the thin leading edge. It was operated by a constant temperature anemometer (CTA) called signal conditioner #1 (Fig. 3). This was custom developed for this experimental airplane (by Kyowa Electronic Instruments Co., Ltd.). The hot film was operated at an overheat temperature of 220°C. The CTA was designed to begin supplying bridge power when the experimental aircraft separated from the rocket at its highest altitude, so that the sensor would never be destroyed by rapid environmental temperature variations on launch. To sense high-frequency fluctuations accurately, ac outputs over 10 Hz and under 10 kHz were separated from dc outputs under 100 Hz, and amplified with 60 times gain. This ac gain was determined based on the estimation of the flight data through the wind-tunnel test as described next. Electrical noise is reduced to about 1 mV_{rms}.

The dynamic pressure transducer measures surface pressure and its fluctuation with a high-frequency response as well as the HF. The transducer was a semiconductor strain gauge type (Kulite Corp. XB44-093) and a 0.7BAR-differential type (Fig. 1). The pressure amplifier to operate this pressure transducer was also custom developed by Kyowa, and is called signal conditioner #2 (Fig. 3). The output was separated into dc outputs under 100 Hz, and ac outputs over 10 Hz and under 10 kHz, which is similar to the HF output. The dc and ac output were amplified with a 140 and 100 times gain, respectively. The dc gain of DP was also determined based on the estimated flight data obtained from the wind-tunnel test as described next. Electrical noise was reduced to about 6.7 Pa_{rms}.

The dc and ac outputs of the HF and the DP were pulse code modulated by signal processors (Fig. 3). They were then recorded in the data recorders with 12 bit, 250 Hz sampling for the dc output, and 10 bit, 20 kHz sampling for the ac output. The dc output is also transmitted to the control center using a telemeter system.

Thermocouple

In general, properties of the heat transfer by convection depend on the flow conditions. This means that the heat transfer coefficient of the laminar flow is different from that of the turbulent flow. The differences in the heat transfer coefficient of the flow induce different temperature variation on the wall with time. Thus, the thermocouple is a useful tool for detecting the boundary-layer transition locations, because the temperature variation on the airplane surface has different behaviors when the flow is laminar and turbulent.

Type-K and ungrounded coaxial thermocouples (Okazaki Manufacturing Co.) were mounted on the NEXST-1 (Fig. 1) and a zero point reference box fitted on the fuselage. To guard against electric and magnetic noise from the signal cable, double shielded cables were used on most sections of the signal lines. Measured analog data were amplified and converted to digital data by a signal processor (Fig. 3).

Preston Tubes

Ten Preston tubes were mounted on the upper surface of the wing. As is well known, the velocity profile on the laminar boundary layer is different from that on the turbulent boundary layer. Because

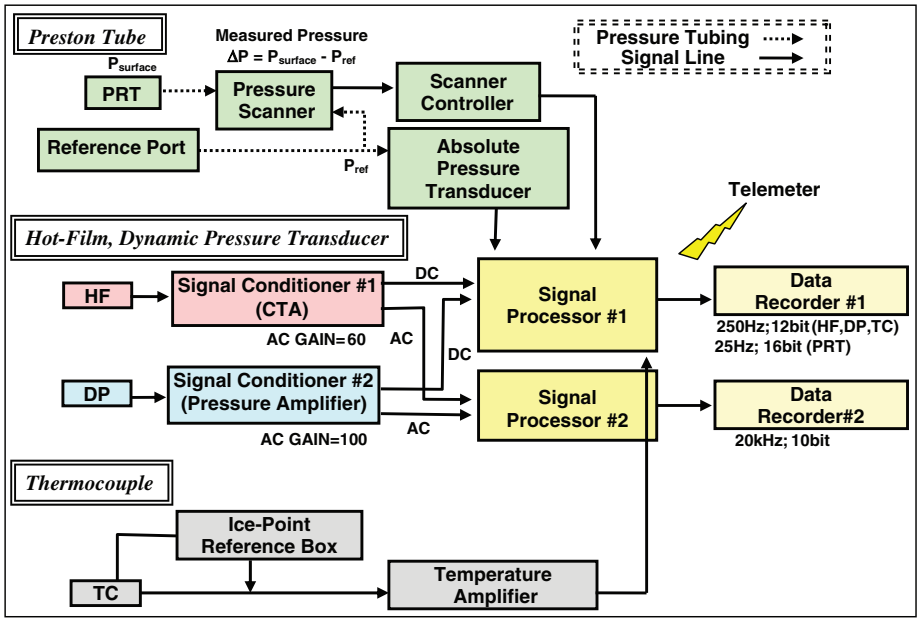

Fig. 3 Flow chart of transition measurement system.

Preston tubes measure local total pressure near the surface, measured total pressure is different from the flow conditions. Therefore, Preston tubes can detect the boundary-layer transition locations. The cross section of the Preston tube tip is rectangular and rounded (Fig. 1). The inner and outer diameter is 0.15 and 0.4 mm in the minor axis, and the inner diameter in the major axis 1.15 mm. These scales are determined from two CFD results in which the state of boundary layer is assumed to be laminar or turbulent, respectively. The results suggested that the difference between laminar and turbulent states can be classified, even at the sensor location where the boundary layer becomes most thin ($X/C = 0.15$, $Y/S = 0.77$) on the main wing of NEXST-1.

The pressure measurement system of the Preston tube is the same as the system of surface pressure measurement [17,18] (Fig. 3). Seven differential-type pressure scanners (ZOC 33, Scanivalve Corp.) are fitted to the fuselage for surface pressure measurement. A pressure port for the reference pressure is installed near the nose. The reference pressure is connected to each pressure scanner (for the backpressure) and an absolute-type pressure transducer (CAT-130-1, Tokyo Aircraft Instrument Co., Ltd.). The reference pressure is nearly equal to the freestream static pressure, allowing measurement ranges of the differential-type pressure scanner to be set to suitable ranges. This system improves the accuracy of the surface pressure measurement. The estimated overall uncertainty of the pressure coefficient C_P is less than ± 0.0115 at 100:1 odds. A number of system checks were conducted to maintain a high degree of reliability in the pressure measurement system.

Preliminary Ground Test

Transition Measurement System

Wind-Tunnel Tests

A wind-tunnel test was performed to check the function of the transition measurement system and to estimate the data obtained in the flight test. To achieve these purposes, the same sensors and amplifiers as those actually mounted on the NEXST-1 were used in the wind-tunnel test, although the gain in ac output of the CTA was 20 times (60 times on the NEXST-1), and the gain in dc output of the pressure amplifier was 350 times (140 times on the NEXST-1). The wind-tunnel test was conducted in an in-draft supersonic wind tunnel, suitable for this type of test because the unit Reynolds number was comparatively close to the flight condition of unit Reynolds number $Re/\mathrm{m} = 12.3 \times 10^6$ (1/m) at $M = 2.0$, and the pressure fluctuation in the uniform flow was very low at $Cp_{\mathrm{rms}} = 0.04\%$. The model consisted of the front part of a Sears–Haack body ($y = f_{\mathrm{nose}}(x) = A[x/l(1 - x/l)]^{3/4}$, where $l = 2692.308$ and $A = 217.59$), which is the same shape as the nose of the NEXST-1. Although four kinds of sensors were flush-mounted at $X_{\mathrm{tip}} = 250$ mm from the tip, with a 60 deg spacing in the circumference direction, the results shown next were obtained with each sensor placed on the top line by rotating the model in the circumference direction. Because the locations of the sensors were fixed on the model surface and the total pressure of the wind tunnel was uncontrollable at almost atmospheric value, the transition location was detected by means of the continuous variation in angle of attack.

The result is explained as follows. First of all, the variation in average of HF dc output E_{mean} and the fluctuation in HF ac output e' with the angle of attack are shown in Fig. 4. As is clearly indicated by this figure, the average HF dc output decreased gradually and increased rapidly almost stepwise with the angle of attack. Because the variation in HF dc output corresponds to the variation in wall shear stress on the boundary layer from laminar to turbulent, as already mentioned, a low-average dc output corresponds to low wall shear stress on the laminar boundary layer. On the other hand, a high average shows the boundary layer to be turbulent with high wall shear stress. Therefore, the stepwise increasing in HF dc output corresponds to the laminar-to-turbulent transition of the boundary layer. Meanwhile, the fluctuation in HF ac output also varied corresponding to variations in dc output. The amplitude of fluctuations in ac output was very small before the dc output began to grow, and was moderate after the dc output reached a high value; furthermore, it was at a maximum between these two states. Because the fluctuation in ac output is known to be small in the laminar state

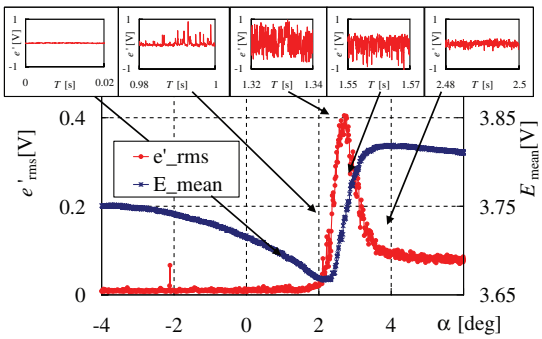

Fig. 4 Variation of HF dc and ac outputs with angle of attack and corresponding time traces on top line of Sears–Haack body measured in wind-tunnel test.

and larger in the turbulent state, the state of the boundary layer is easily estimated from the fluctuation in ac output. It corresponds to that estimated from the average of dc output. The variation in ac output, however, shows earlier onset and later end of transition than those detected from the dc output; the fluctuation in ac output tends to detect the boundary-layer transition more sensitively. Incidentally, the variation in fluctuations in the HF ac output, reaching its maximum between the laminar and turbulent states, is caused by typical variations in instantaneous time traces, and does seem to relate to the occurrence of turbulent spots (Fig. 4). At the beginning of the transition process, the fluctuation in HF ac output increased corresponding to the occurrence of the positive spike signal in the time trace. This could be caused by an instantaneous increase in dc output in line with the passage of turbulent spots. As the transition process progresses, and as turbulent spots occur more frequently, the fluctuations in ac output increase. After the peak of the fluctuation, the local laminar region remains in the turbulent boundary layer, and then negative spike signals seem to occur. Such variations in the fluctuation and time trace of the HF ac output were observed, not only on the transition in the compressible boundary layer, but also in the low subsonic flow [19,20]. These values are expected to help in clarifying the boundary-layer state in transition detection, acting as an effective guidepost.

The fluctuations in DP ac output p' with the angle of attack, similar to the HF ac output, are plotted in Fig. 5. The variation in instantaneous time trace was also found to be similar to the HF output. Although the upward or downward spike signal was not as significant as the HF ac signal, the skewness, which is positive at the beginning of the transition and negative at the end, is the same. Therefore, the variation in the time trace of the DP ac output is also regarded as a significant guidepost for detecting the transition.

A time trace of the surface temperature T_{TC} measured by the thermocouple is shown in Fig. 6. In the case of α sweep (in which the angles of attack increase continuously from −4 to 6 deg), a time trace of temperature and corresponding variation in angle of attack α are shown by the purple and pink lines, respectively. In this case, the temperature gradient has a constant value until $T_{blow} = 6$ s, and then the gradient changes to another value. The angle of attack, which corresponds to the change in the temperature gradient, is $\alpha = 2.8$ deg. The time trace of the temperature in the case of α constant ($\alpha = 0$ and 5 deg) was also plotted in Fig. 6. The temperature gradient on $\alpha = 0$ deg (orange line) corresponded with that observed at $\alpha < 2.8$ deg of the α-sweep case. A similar tendency was observed on $\alpha = 5$ deg (yellow line) and $\alpha > 2.8$ deg of the α-sweep case, meaning that the gradual temperature gradient observed at $\alpha < 2.8$ deg was induced by the laminar flow, whereas the steep gradient observed at $\alpha > 2.8$ deg was induced by the turbulent flow in the α-sweep case. A higher heat transfer coefficient in turbulent flow induces a higher gradient of temperature than the laminar flow that has a lower heat transfer coefficient. The detection of the boundary-layer transition locations on the flight test by means of the thermocouple was confirmed from the wind-tunnel test that simulated the α-sweep phase on the flight test.

Figure 7 shows variations in the local total pressures P_{PRT} measured by the Preston tubes in the wind-tunnel test. Preston tubes were mounted at different distances from the tip X_{tip}. The inner diameter in minor axes of all tubes is 0.1 mm. This height is also examined based on CFD analysis. The results suggested that the difference between laminar and turbulent states can be classified at each sensor location. With increasing angles of attack, the transition location on the top of the model moves forward. Therefore, the sensor located further forward will measure the laminar flow during the width range of α more than the sensor in a more rearward location. The abrupt change of the pressure observed at $\alpha = 2 \sim 3$ deg on the Preston tube located at $X_{tip} = 250$ mm (illustrated by the green line in Fig. 7) was generated by the boundary-layer transition. On $\alpha < 2$ deg, the flow is laminar at the sensor location, then the Preston tube measures lower pressure than turbulent regions. When the angles of attack increase within the laminar region, the boundary layer developed with the angle of attack, and therefore the pressure measured by the Preston tube decreased due to the constant height of the Preston tube. The Preston tube located at $X_{tip} = 350$ mm (orange line in Fig. 7) also detected the boundary-layer transition, but transition occurred at a lower angle of attack than at $X_{tip} = 250$ mm. At the more rearward locations, namely $X_{tip} = 400$ mm and $X_{tip} = 450$ mm, the Preston tube did not detect the transition and indicated that the boundary layer was turbulent during the measurement.

Outputs of all four sensors at the same location from the tip $X_{tip} = 250$ mm were superimposed and compared (Fig. 8). In the results, the angles of attack where the boundary-layer transition was detected by each sensor are in good agreement. Because it was confirmed by the wind-tunnel test that the transition location can be detected consistently in the supersonic boundary layer using four kinds of sensors, the output levels at laminar and turbulent states for HF and DP could be estimated. As mentioned, the unit Reynolds number and pressure fluctuation in the uniform flow are expected to be close to the flight condition, and the sensitivity for those quantities is not clear, and so we estimate the values obtained in the wind-tunnel test to be almost identical to those obtained in the flight test. The gain of the amplifier was then regulated.

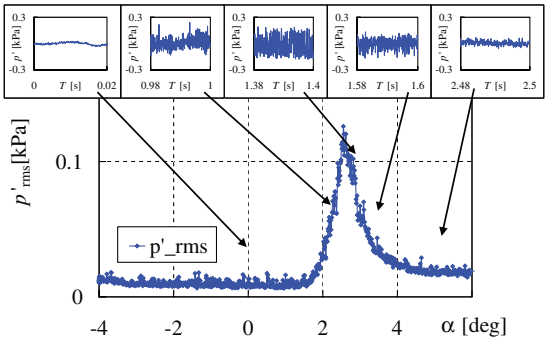

Fig. 5 Variation in DP ac output with angle of attack and corresponding time traces on top line of Sears–Haack body measured in wind-tunnel test.

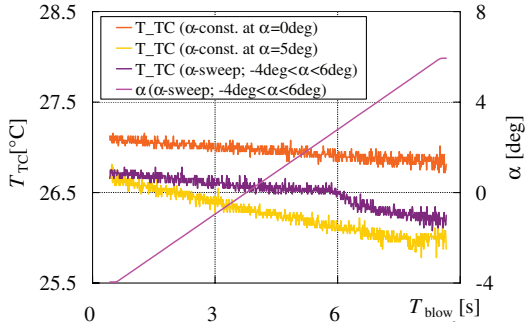

Fig. 6 Time traces of TC output on top line of Sears–Haack body measured in wind-tunnel test.

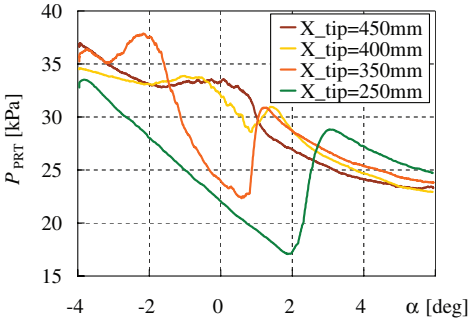

Fig. 7 Variation in local total pressure measured by PRT with angle of attack and corresponding time traces on top line of Sears–Haack body measured in wind-tunnel test.

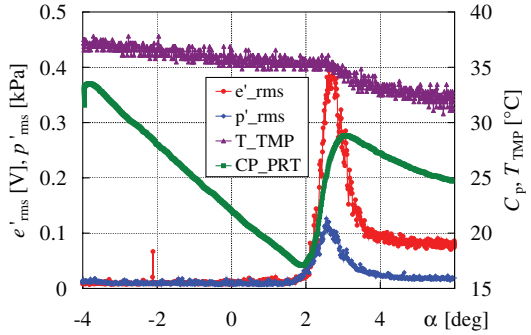

Fig. 8 Comparison of outputs of all four kinds of sensors at $X_{tip} = 250$ mm obtained in wind-tunnel test.

The uncertainty of the pressure coefficient measured by the Preston tube was obtained from the pressure measurement system of the NEXST-1 [17,18]. The uncertainty due to pressure response delay by the tubing was also added to the overall uncertainty. The estimated overall uncertainty of the pressure coefficient C_P is less than ± 0.0115 at 100:1 odds. A number of checks were conducted to ensure a high level of reliability in the pressure measurement system before and after the flight test.

Function Test Onboard

Other tests to examine instrument function were performed on the ground. Actual accuracy of DP ac output was checked by absorbing pressure from each sensor directly. From a number of measurements, it was confirmed to be 6.7 Pa_{rms}, which corresponds to 1 bit.

Functions of all instruments and electromagnetic interference were tested under conditions in which all were mounted on the NEXST-1. All data acquired through these tests were analyzed each time to find abnormal output as early as possible, and all four sensors were confirmed to be in normal condition right up to just before the launch.

Natural Laminar Flow Wing Concepts

NLF concepts were preliminarily examined through a series of wind-tunnel tests. One series of tests was performed using a half-model of 15.7% scale of the NEXST-1 in the aforementioned in-draft supersonic wind tunnel [14]. The Mach number M was 2.0, the same as for the flight experiment, although the Reynolds number Re_c was 4.6×10^6, much lower than the flight experiment. A multi-hot-film sensor was used to obtain the transition location on the main wing. Although the disturbance growth in the boundary layer was observed, the transition location defined at the peak location of disturbance did not detect up to the most downstream sensor location $X/C = 0.5$ at angle of attack $\alpha = 2.7$ deg, where the surface pressure distribution was in good agreement with designed distribution. Therefore, it seems that NLF wing concept was achieved.

A second series of tests was performed using a 23.3% scaled model at the S2MA (ONERA) [14]. The Mach number M was also 2.0, the same as the flight experiment. The Reynolds number Re_c was up to 10.7×10^6. This value is almost half of the flight experiment condition, and the highest in these wind-tunnel tests. A hot-film sensor and infrared camera were used to obtain the transition location. The detected transition location depended on the angle of attack. The transition location at the inner wing was most delayed at the design point $\alpha = 2$ deg, although the location at the outer wing was most delayed at the larger angle of attack. This discrepancy was explained by the difference in the surface pressure distributions. Because an adverse pressure gradient hardly occurred at the positive angle of attack and the acceleration became rapid near the leading edge at the outer wing, not only T-S instability but also crossflow instability were suppressed. This tendency was in good agreement with numerical predictions.

Another series of wind-tunnel tests was performed using a model of 8.5% scale of the NEXST-1 [21]. The tests were conducted in a 1×1 m JAXA supersonic wind tunnel at $M = 2.0$. The Reynolds number Re_c was 6.3×10^6. The transition location on the upper surface of the wing was measured by the Preston tube, although the Preston tube of the wind-tunnel model had a different height and width from the Preston tube of the NEXST-1. When the α changed from -3 to 8 deg, a region in which the C_P has a lower value than the other regions was observed at around $\alpha = 2$ deg. As mentioned, the region in which the C_P has a lower value corresponded to the laminar boundary layer. The laminar flow region decreases when the chordwise locations of the Preston tube move to rearward locations. These results mean that the boundary-layer transition locations on the $\alpha = 2$ deg moved to a more rearward location than that on the other α. In other words, the largest laminar region was achieved at a design point of the NEXST-1.

The propriety of the aerodynamic design on the NLF wing was confirmed qualitatively in all the wind-tunnel tests. However, the Reynolds number and the level of freestream fluctuation in the wind-tunnel test conditions are different from the flight test conditions. Therefore, a quantitative evaluation will be performed from the NEXST-1 flight experiment.

Results of the Flight Experiment

Outline of Flight Experiment

Because the details of the NEXST-1 flight experiment are presented in [2,3], we just give a brief outline here (Fig. 2). NEXST-1 is a vehicle of total length 11.500 m, full span 4.718 m, and total weight including all components of 1940.7 kg [3,15]. The wing and the nose surface were polished to the same level as a transition model for wind-tunnel testing, because external disturbances which can lead to transition must be excluded. The surface roughness was measured using a laser displacement measurement system. The polishing requirement is below 0.3 μm in arithmetical mean deviation, although the practical value was below 2 μm.

This flight experiment was successfully conducted at the Woomera Prohibited Area in South Australia. The NEXST-1 was launched on 10 October 2005 by a solid rocket booster in piggyback form, as shown in Fig. 2. After the separation from the rocket booster at an altitude of $H \approx 19$ km and $M \approx 2.3$, the NEXST-1 flew at supersonic speed like a glider through two successive test phases. During the flight, more than 500 technical data, such as aerodynamic force, surface pressure [17,18], and boundary-layer transition, were acquired at Mach number $M \approx 2$. After the test phase, the NEXST-1 was recovered on the ground by parachutes and air bags. Most measurement data are downlinked to the ground facility by real-time telemetry systems. Simultaneously, all the measured data are recorded to a data recorder onboard the NEXST-1.

The first of the two test phases is called the "α-sweep" test phase, in which the angle of attack α was controlled to obtain six values for specific lift coefficient C_L including the design point [3,15,22,23]. At the fourth step, the lift coefficient had the design value $C_L = 0.10$. The angle of attack was held during about 4 s in each step because of the requirements of the pressure measurement system [17,18]. After the α-sweep test phase, the NEXST-1 descended rapidly to recover a Mach number, then entered the second test phase. The second test phase is called the "Re-sweep" test phase, in which NEXST-1 glided in, keeping a constant lift coefficient at the design point ($C_L = 0.10$). The variation in the Reynolds number Re_c based on the mean aerodynamic chord at the Re-sweep test phase was from 34.3×10^6 to 35.2×10^6, and therefore not significant because of a shorter flight time than that of our estimation. The largest variation in Re_c, however, was obtained when the Re_c values between the Re-sweep test phase and the fourth step of the α-sweep test phase were compared. The Reynolds number at the fourth step of the α-sweep test phase, $Re_c = 14.9 \times 10^6$, was one-third of that at the Re-sweep test phase. Through the flight experiment, three types of aerodynamic data were measured: 1) surface static pressure distributions, 2) boundary-layer transition locations, and 3) aerodynamic forces to verify the design concepts. All data were obtained successfully. The results of surface pressure measurements and aerodynamic force measurements are summarized in [17,18,22,23].

Transition Measurements at α-Sweep Test Phase

Hot-Film Sensor

The time-series data obtained from the HF were analyzed as follows. First of all, an instantaneous time trace corresponding to each flight test event was obtained and its characteristics considered. Second, a spectrum was obtained by fast Fourier transform analysis. Data with 4096 points were obtained, with a 1024 point shift, and these spectrums averaged 16 times. Then, the time average, rms value, skewness, and maximum and minimum value for each 0.4 s were obtained to evaluate the statistical variation in outputs. In the following, our attention focuses on the time-averaged dc output and the rms value of ac outputs. First of all, to detect transition location, let us consider the variation in the average dc output and fluctuation in the ac output at a chordwise position normalized by the local chord length $X/C = 0.25$ and $Y/S = 0.31$ in the α-sweep test phase shown in Fig. 9 as typical results. Variations in lift coefficient C_L are also plotted in the same figure to give a clear comparison between HF output and the flight condition of the NEXST-1 by the sweep of angle of attack. The average HF dc output increased steeply from $E_{\text{mean}} = 3.54$ V to $E_{\text{mean}} = 3.59$ V, at the time from liftoff $T_{\text{lo}} = 105$ s, when the α-sweep test phase began and lift coefficient was $C_L = -0.01$. It then decreased rapidly to almost the same value as at the beginning, $E_{\text{mean}} = 3.55$ V at $T_{\text{lo}} = 118$ s, when the flight condition changed from the third step of the α-sweep test phase ($C_L = 0.07$) to the fourth step of $C_L = 0.10$. Then, thirdly, it began to gradually increase at $T_{\text{lo}} = 123$ s, when the flight condition changed from the fourth step to the fifth step of $C_L = 0.14$, and overshot when the lift coefficient settled at the fifth step. Finally, at the sixth step ($C_L = 0.17$), the average of the HF dc output settled at $E_{\text{mean}} = 3.61$ V, almost the same value as the first to third steps. As already mentioned, the average of the HF dc output is known to be low in the laminar region and high in the turbulent region. Such variations were confirmed in the wind-tunnel test. Consequently, the boundary layer at the sensor location is considered to be laminar at the fourth step of $C_L = 0.10$, turbulent from the first step to the third step, and at the sixth step, and a transitional state between laminar and turbulent at the fifth step.

The fluctuations were very small in $e'_{\text{rms}} \approx 0.02$ V at the fourth step of the α-sweep test phase between $T_{\text{lo}} = 119$ and 122 s, when the boundary layer is interpreted as being laminar from the HF dc output. The fluctuations were very large before and after the fourth step when it corresponds to the third and fifth step. The fluctuations at the first, second, and sixth steps settled at the comparatively large value $e'_{\text{rms}} \approx 0.24$ V. These variations correspond closely to the variation from laminar to turbulent observed in the wind-tunnel test. Therefore, the boundary layer is supposed to be laminar at the fourth step, turbulent at the first, second, and sixth step, and in a transitional state at the third and fifth step. The variation in the state of the boundary layer, inferred from the fluctuations in the HF ac output, agrees qualitatively with that inferred from the average of the HF dc output. Inconsistency is, however, observed at the third step in a strict sense. The boundary layer is inferred to be turbulent from the HF dc output average, but in a transitional state from the fluctuations in HF ac output. To confirm the state of the boundary layer, assumed from the average HF dc output and the fluctuations in HF ac output, an instantaneous time trace and spectrum must also be examined. The time trace during 0.03 s, when the flight condition settles at typical step, is shown in the same figure. The time traces of the first, second, and sixth step seemed to resemble each other, and to be random noise. On the other hand, at the third and fifth steps, a spike signal was observed. These time traces are evidence of the fact that the boundary layer is in a transitional state near turbulent, as confirmed from the wind-tunnel test. Then, at the fourth step, the amplitude of the time trace was very small and shows that the boundary layer is laminar. These facts are also clear from the spectrum. As a conclusion, the state of the boundary layer clarified from the time trace is confirmed to coincide with the state interpreted from the average HF dc output and the fluctuation in HF ac output.

Dynamic Pressure Transducer

Next, let us consider the fluctuating output of DP. As already mentioned, our attention is paid only to the ac outputs. The data were analyzed in the same manner as HF.

From the aforementioned wind-tunnel test, it was confirmed that fluctuations in DP ac output varied coinciding with the HF ac output. The variation in the fluctuation in DP ac outputs shown in Fig. 10 seems at first glance to be similar to the fluctuations in HF ac output shown in Fig. 9. At $X/C = 0.20$, the fluctuation at the fourth and fifth step was also very small, and the boundary layer is interpreted to be in a laminar state. Though the fluctuation in DP ac output was large with $p'_{\text{rms}} \approx 0.02$ kPa under another condition, from the first to third step, and at the sixth step, the boundary layer at the second and third step is supposed to be in the transitional state. At the first and sixth step, it is supposed to be in a turbulent state because the fluctuation in the second and third steps was slightly larger than that on the first and sixth steps, and a very large peak was observed at $T_{\text{lo}} = 115$ s between the second and third steps, as well as in the wind-tunnel test. A similar peak was also observed at $T_{\text{lo}} = 127$ s between the fifth and sixth steps, though the amplitude was relatively small.

The instantaneous time traces at $X/C = 0.20$ are examined to confirm the state of the boundary layer inferred from the fluctuations in DP ac output, in the same way as the HF outputs, as shown in the same figure. The characteristics of the time traces from the first to third step, and at the sixth step, and those at the fourth and fifth steps, resemble each other. First, the time traces of the fourth and fifth step are compared. The amplitude of the fifth step was found to be larger than that of the fourth step. Although there was a difference in the amplitude, the amplitude in the high-frequency spectrum component decreased with frequency, and the boundary layer is confirmed to be in a laminar state for both conditions. Next, the time traces from the first to third step and at the sixth step are compared. At the second step, downward spike signals occurred, although the amplitude was much smaller than that of the HF output. On the other hand, upward spikes occurred at the third step. Moreover, no spike signal was observed at the first and sixth steps. Therefore, from the fluctuations, it can be concluded that the boundary layer is in a transitional state at the second and third steps, and at a turbulent state at the first and sixth steps.

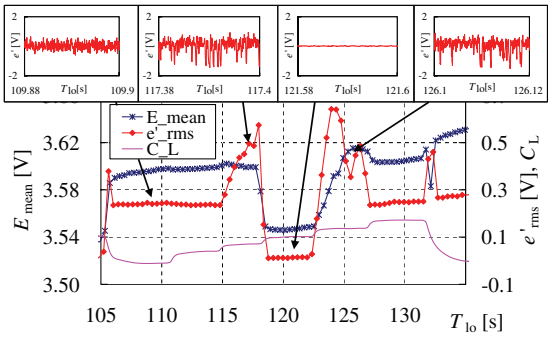

Fig. 9 Variation in HF dc and ac outputs with angle of attack and corresponding time traces in flight test.

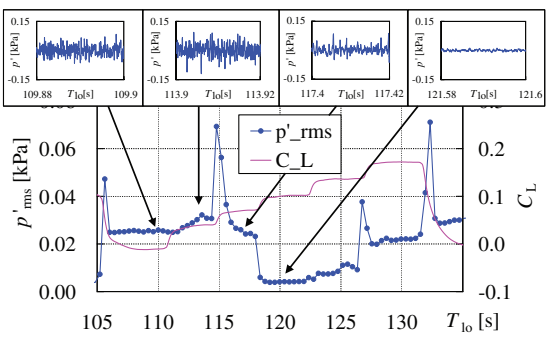

Fig. 10 Variation in DP ac output with angle of attack and corresponding time traces in flight test.

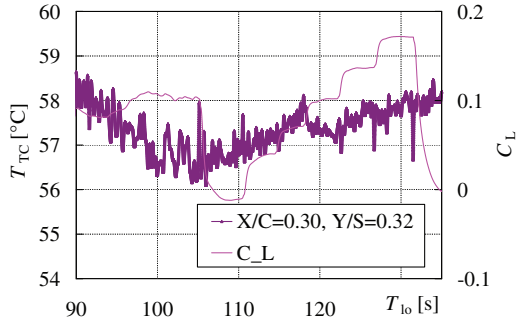

Fig. 11 Variation in surface temperature measured by thermocouple with angle of attack in flight test.

Thermocouple

A typical result of local temperature T_{TC} measured by the thermocouple is shown in Fig. 11. T_{TC} is found to vary slightly corresponding to the change in lift coefficient. In Fig. 11, the temperature gradient at the fourth step of the α-sweep test phase between $T_{lo} = 119$ and 122 s clearly corresponds to the gradient before the α-sweep test phase ($T_{lo} < 105$ s). Because the lift coefficient before the α-sweep test phase agrees with the value at the fourth step, the agreement in temperature gradient is reasonable. In contrast, the gradient of T_{TC} at the other steps is almost constant, and is completely different from that at the fourth step. This result indicates that the thermocouple detected the boundary-layer transition, and that the state of the boundary layer at the fourth step is different from that at the other steps.

As illustrated, the temperature gradient varies with the state of the boundary layer. In the wind-tunnel test, the temperature gradient in the turbulent state was higher than that in the laminar state, but the sign of both gradients was the same. In contrast, the temperature gradient sign in the two states is different in the flight test, because the temperature gradients depended strongly on the recovery temperature and on the wall temperature of the no-adiabatic airplane surface. Moreover, the flow conditions are completely different. Because the wind tunnel is of the in-draft type, the supersonic flow condition is already achieved, but the surface temperature on the no-adiabatic model is still transient from the no-wind condition to the supersonic condition in the wind-tunnel test. In contrast, sufficient time has passed from the supersonic condition being achieved to the test phases in the flight test. Therefore, the variation in surface temperature in the flight test is less than that in the wind-tunnel test. The boundary-layer transition can be detected by the thermocouples. However, the temperature gradient had hardly changed, and the state of the boundary layer was interpreted with assistance from the result of the other three sensors near the thermocouple under consideration or remained open to question.

Preston Tube

Figure 12 shows the variations in the pressure coefficients C_p on the α-sweep test phase measured by the Preston tube at different locations, with the variation in C_L. C_p is defined as the difference between the local total pressure measured by PRT and the static pressure of freestream normalized by the dynamic pressure of freestream.

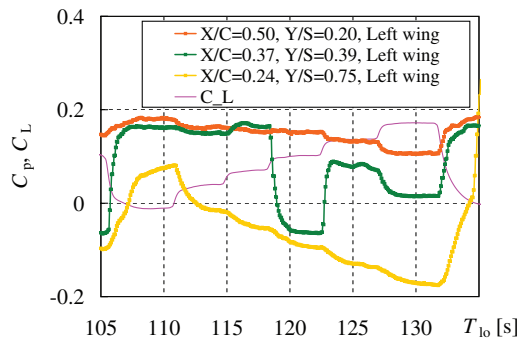

Fig. 12 Variation in C_p obtained by Preston tube with angle of attack in flight test.

At the α-sweep phase, variations in the C_p at each location can be classified into two types. One type of C_p variation was very slight, such as that at $X/C = 0.24$, $Y/S = 0.75$ (yellow line) and $X/C = 0.50$, $Y/S = 0.20$ (orange line). The absolute value of C_p was divided into two groups, with lower values such as $X/C = 0.24$, $Y/S = 0.75$ (yellow line) and higher values such as $X/C = 0.50$, $Y/S = 0.20$ (orange line). The other type of variation shows a sudden, large change in C_p, such as that at $X/C = 0.37$ and $Y/S = 0.39$ (green line). The C_p was low at the fourth step on the α-sweep test phase, that is, the design point, and high at other steps. A similar tendency to this type of C_p variation was also observed in the wind-tunnel test as mentioned earlier (Fig. 7). The C_p was low at the fourth step and some other steps near the fourth step. These results suggest that the sudden and large change in C_p was induced by the boundary-layer transition. Also, the low and high values of C_p are considered to correspond to the laminar and turbulent state, respectively.

To confirm the state of the boundary layer, a simple estimation of the C_p measured by the Preston tube was conducted using the CFD analysis results [24,25]. Because the details of the estimation are presented in [21], just a summary is provided here. Flow conditions (boundary-layer thickness and local velocity, surface pressure, density) at the end of the boundary layer were obtained from the Navier–Stokes CFD analysis [24,25] on the laminar flow and fully developed turbulent flow conditions. To simplify the estimations, the laminar boundary-layer profiles at all locations and all α is assumed to be as same as the typical profile of the laminar boundary layer at $M = 2$, $\alpha = 2.0$ deg, $Y/S = 0.20$, $X/C = 0.50$. This assumption is able to be used because the boundary-layer profiles vary only very slightly with the chordwise and spanwise locations on the wing and the altitude, and the variation in boundary-layer profile on the locations and the α is negligible. The turbulent boundary-layer profiles at each location were also obtained from the same assumption. Then, C_p at each location was calculated. The results showed the estimated C_p of the laminar flow to be lower than that of the turbulent flow. The estimated C_p of the laminar boundary layer, moreover, is very close to the experimental results obtained at $X/C = 0.24$, $Y/S = 0.75$ (yellow line in Fig. 12), where the boundary layer is considered to be laminar. However, the estimated C_p of the turbulent boundary layer is slightly lower than the experimental values obtained at $X/C = 0.50$, $Y/S = 0.20$ (orange line in Fig. 12), where the boundary layer is considered to be turbulent, and the qualitative tendency of the estimated C_p is in good agreement with the experimental results. Therefore, it is concluded that our interpretation of the state of the boundary layer measured by the Preston tube in the flight test is correct.

Validation of Natural Laminar Flow Wing Concept

Transition Location

Typical results obtained by use of all four types of sensors and during the test phase (before the α-sweep test phase to the end of the Re-sweep test phase) are superimposed in Fig. 13. The outputs obviously varied with lift coefficient (in other words, angle of attack) during the α-sweep test phase. However, this was quite gentle during the Re-sweep test phase and between the two phases. On the Re-sweep test phase and between the two phases, the state of the boundary layer at each sensor location is interpreted in the same manner as that in the α-sweep test phase. For example, all outputs shown in Fig. 13 indicate that the boundary layer at each location is turbulent on the Re-sweep test phase and between the two phases.

The transition location distributions are defined at the end of transition according to objective criteria [21,26]. Especially for HF dc, HF ac, and DP ac, we here introduce the new notion of a "transition level" based on the following criterion, and try to determine the state of the boundary layer in both objective and subjective terms. An explanation of the method for determining the transition level, based on average dc output, is as follows. First, the variation in time of the absolute value of average the dc output for the

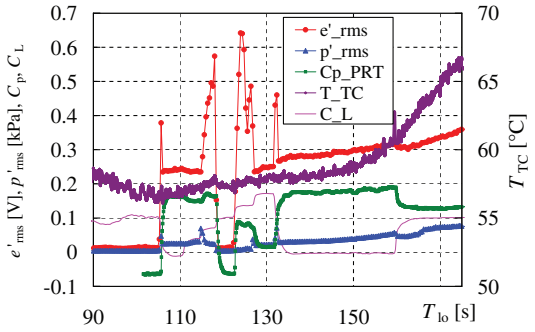

Fig. 13 Comparison of all sensor types in flight test.

two regions, where the boundary is regarded as laminar and turbulent, is approximated by a linear function, respectively. Next, the difference between two approximated values for laminar and turbulent states is equally divided into six, and the dc output measured from the experiment is compared with each divided value. The transition level is defined as the closest criterion to the experimental data, in order, from "one" corresponding to the laminar criterion, to "seven" corresponding to the turbulent criterion. The explanation of the method for determining the transition level, based on the fluctuation in ac output, is as follows. First, the variations in time of the absolute value of the fluctuation in ac output for the two regions, where the boundary is regarded as laminar and turbulent, are approximated by a linear function, respectively, as well as dc output. Next, the difference between the two approximated values in the laminar and turbulent states is equally divided into two, and fluctuation in excess of the turbulent state is also divided by the same interval by extrapolating from the turbulence level. Then, the skewness is examined, because the fluctuation is at a maximum in the transitional region and takes the same value at the beginning of the transitional state as turbulence states. If the skewness is positive, the transition level is defined as from one (corresponding to the laminar state) to "four" depending on the absolute value of the fluctuation in ac output. Otherwise, the transition level is defined as from "six" to seven (corresponding to the turbulent state). When the fluctuation is near the maximum, the transition level is defined as "five."

As a typical case, those at the second and fourth steps of the α-sweep test phase and Re-sweep test phase are shown in Figs. 14a–14c, respectively. BP of the ordinate is buttock plane and FSTA of the abscissa is the fuselage station. The state of transition was classified into two conditions. One is the laminar or transitional state (plotted in blue symbols), and the other is the turbulent state (plotted in orange symbols). The shapes of the symbols indicate the types of sensor. As mentioned earlier, the state of the boundary layer measured by some thermocouples remained an open question. Such locations are plotted in white symbols. Especially in the Re-sweep test phase, the state of the boundary layer measured by some thermocouples was not determined, because the temperature gradients varied only very slightly with the Reynolds number.

It is clear that the transition location at the fourth step of the α-sweep test phase (Fig. 14b) at $C_L = 0.10$ moves much further downstream than the location at the second step (Fig. 14a) at $C_L = 0.04$, and that the natural laminar flow effect appears on the wing. Furthermore, the transition location of the Re-sweep test phase is compared with the α-sweep test phase, with the same lift coefficient $C_L = 0.10$ at the design point. Because the altitude of $H = 12.2$ km in the Re-sweep test phase at $T_{lo} = 167$ s is much lower than that of $H = 18.1$ km in the fourth step of the α-sweep test phase, the corresponding Reynolds number based on the mean aerodynamic chord $Re_c = 34.3 \times 10^6$ in the Re-sweep test phase is higher than that of $Re_c = 14.9 \times 10^6$ in the α-sweep test phase. As a result, the transition location moves much further forward. From this result, the natural laminar flow effect at the design point (namely, $C_L = 0.1$ at $M = 2.0$ and $H = 18$ km) is obvious (Fig. 14c).

It is confirmed that this suppression of transition is caused by the achievement of target surface pressure distribution from the results in the flight test [17,18]. The surface pressure distribution is in good

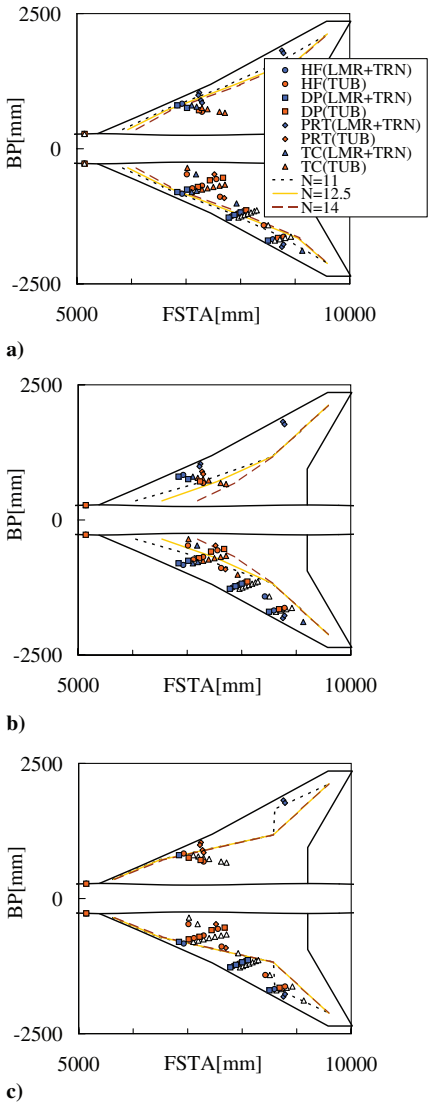

Fig. 14 Transition location distribution. Comparison with transition level obtained from experimental result and numerically predicted N value.

agreement with the CFD results [24,27], including the effects of aeroelastical deformation, revision related to the angle of sweep, and so on, to simulate the flight condition exactly [22]. A steep increase at the leading edge of the pressure distribution, on the upper surface at the design point, was observed at the fourth step of the α-sweep test phase, meaning the growth of crossflow instability is suppressed. A following gradual increase in the trailing edge was also observed, meaning no adverse pressure gradient region was observed, and T-S wave-type instability was also suppressed. On the other hand, at the off-design point, for example, in the second step of the α-sweep test phase, though the favorable pressure gradient region was quite narrow, it is followed by an adverse pressure gradient region. Therefore, T-S wave-type instability is not supposed to be suppressed sufficiently.

Numerical Prediction

Because the natural laminar flow effect was confirmed from the experimental data, the effect was then compared with the numerical prediction [11–13,28]. As is well known, the transition location is generally predicted according to the following four steps. First, the surface pressure distribution is obtained. Then, as the second step, the laminar boundary-layer profile is calculated. Then, the stability of the boundary layer is analyzed as the third step, and the growth rate is integrated as the last step. For the present prediction, the boundary-layer profile was calculated using the conical flow approximation of

Kaups–Cebeci, based on the surface pressure distribution experimentally measured during the flight test [17,18]. Then, the stability of the boundary layer is analyzed by the LSTAB, explained in the Introduction. The growth rate is also integrated along the external streamline, applying the envelope strategy [11–13,28]. However, if the iso-N value line appeared in the downstream region after $X/C = 0.6$, we assumed that the amplification of the disturbance was fixed at $X/C = 0.6$ in the transition prediction, because it was not easy in practical terms to maintain the laminar boundary layer after $X/C = 0.6$ due to the existence of the control surface.

The resultant predicted transition locations at the second and fourth steps of the α-sweep test phase and Re-sweep test phase are superimposed in Fig. 14 as the iso-N value line. When the transition locations obtained experimentally and numerically were compared, the experimental location was found to be in good agreement with the iso-N value line at $N = 12.5$ on the inner-wing region of $Y/S \leq 0.6$ in all cases, including these three. This N value was smaller than the specific value of $N = 14$ obtained through the wind-tunnel result at NASA [29], although notable discrepancies were observed in the outer-wing region. This disagreement is supposed to be caused by the discrepancy in the boundary-layer profiles, because it has been found out that trial analysis by Navier–Stokes calculation to obtain the boundary-layer profile yields a different transition pattern from the present results [28]. Moreover, other trial analysis based on the calculated surface pressure distribution by Navier–Stokes analysis also yields a different boundary-layer profile and transition pattern from both transition patterns mentioned previously. Therefore, when the numerical method of Navier–Stokes calculation is improved, the predicted transition locations are expected to agree better than the present results.

In the present analysis, the transition location detected experimentally can be determined as in good agreement with the numerical prediction qualitatively at least, based on accordance in the inner-wing region. Therefore, it is concluded that the natural laminar flow effect was confirmed at the design point $C_L = 0.10$, where the transition location moved much further downstream than the off-design point $C_L = 0.04$.

Conclusions

Flight test of the supersonic experimental airplane NEXST-1 was successfully performed by the Japan Aerospace Exploration Agency to validate advanced aerodynamic design technology. To verify the natural laminar flow wing concept, a high-quality transition measurement system was constructed. The function of this measurement system was examined through preliminary tests on the ground. Using the system, numerous valuable experimental data were obtained in the supersonic flight test. Variation in signals corresponding to the laminar-to-turbulent transition process was observed in the transition measurements. The state of the boundary layer at each sensor location was classified according to objective criteria and the transition location distribution obtained for each time. The natural laminar flow effect was confirmed at the design point $C_L = 0.10$, where the transition location moved much further downstream than the off-design point $C_L = 0.04$.

Acknowledgments

The authors are deeply indebted to the staff of Mitsubishi Heavy Industries, Ltd., Kawasaki Heavy Industries, Ltd., Kyowa Electronic Instruments Co., Ltd., Ohte Giken, Inc., and Fuji Heavy Industries, Ltd., for their great assistance in making the flight test a success and obtaining aerodynamic measurements. The authors would also like to acknowledge the data analysis assistance and support of H. Ishikawa, Y. Yokokawa, M. Noguchi, F. Kuroda, T. Fujiwara, K. Nakahata, H. Hirano, H. Kawakami, and T. Takatoya of the Japan Aerospace Exploration Agency, and advice on instruments from R. Yanagi and S. Takagi of the Japan Aerospace Exploration Agency, M. Nishioka of Kyoto University, Y. P. Kohama of Tohoku University, and M. Asai of Tokyo Metropolitan University.

References

[1] Sakata, K., "Supersonic Experimental Airplane (NEXST) for Next Generation SST Technology: Development and Flight Test Plan for the Unmanned Scaled Supersonic Glider," AIAA Paper 2002-0527, Jan. 2002.

[2] Ohnuki, T., Hirako, K., and Sakata, K., "National Experimental Supersonic Transport Project," *Proceedings of the 25th Congress of the International Council of the Aeronautical Sciences, 2006-1.4.1* [CD-ROM], Optimage, Edinburgh, Sept. 2006.

[3] Fujiwara, T., Hirako, K., and Ohnuki, T., "Flight Plan and Flight Test Results of Experimental SST Vehicle NEXST-1," *Proceedings of the 25th Congress of the International Council of the Aeronautical Sciences, 2006-6.2.1* [CD-ROM], Optimage, Edinburgh, Sept. 2006.

[4] Yoshida, K., and Makino, Y., "Aerodynamic Design of Unmanned and Scaled Supersonic Experimental Airplane in Japan," *Proceeding of ECCOMAS 2004* [online], http://www.mit.jyu.fi/eccomas2004/proceedings/proceed.html, 2004.

[5] Carlson, H. W., and Miller, D. S., "Numerical Method for the Design and Analysis of Wings at Supersonic Speeds," NASA TN D7713, 1974.

[6] Kuchemann, F. R. S., *Aerodynamic Design of Aircraft*, Pergamon, Oxford, England, U.K., 1978.

[7] Ashley, H., and Landahl, M., *Aerodynamics of Wings and Bodies*, Dover, New York, 1965.

[8] Yoshida, K., "Overview of NAL's Program Including the Aerodynamic Design of the Scaled Supersonic Airplane," *Fluid Dynamics Research on Supersonic Aircraft*, RTO Educational Notes 4, NATO Research and Technology Organization, 1998, pp. 15.1–15.16.

[9] Ogoshi, H., "Aerodynamic Design of a Supersonic Airplane Wing: Application of the Natural Laminar Flow Concept to Airfoil," *Proceedings of the 47th Natural Congress of Theoretical & Applied Mechanics*, Architectural Inst. of Japan, Tokyo, Jan. 1998, pp. 341–342 (in Japanese).

[10] Jeong, S., Matsushima, K., Iwamiya, T., Obayashi, S., and Nakahashi, K., "Inverse Design Method for Wings of Supersonic Transport," AIAA Paper 98-0602, Jan. 1998.

[11] Arnal, D., "Boundary Layer Transition Prediction Based on Linear Theory," AGARD Rept. 793, 1993, pp. 2-1–2-63.

[12] Yoshida, K., Ishida, Y., Noguchi, M., Ogoshi, H., and Inagaki, K., "Experimental and Numerical Analysis of Laminar Flow Control at Mach 1.4," AIAA Paper 99-3655, June 1999.

[13] Ueda, Y., Ishikawa, H., and Yoshida, K., "Three Dimensional Boundary Layer Transition Analysis in Supersonic Flow Using a Navier-Stokes Code," *Proceedings of 24th Congress of the International Council of the Aeronautical Sciences, 2004-2.8.2* [CD-ROM], Optimage, Edinburgh, Aug. 2006.

[14] Sugiura, H., Yoshida, K., Tokugawa, N., Takagi, S., and Nishizawa, A., "Transition Measurements on the Natural Laminar Flow Wing at Mach 2," *Journal of Aircraft*, Vol. 39, No. 6, 2002, pp. 996–1002.

[15] Yoshida, K., Makino, Y., and Shimbo, Y., "Experimental Study on Unmanned Scaled Supersonic Experimental Airplane," AIAA Paper 2002-2842, June 2002.

[16] Tokugawa, N., Kwak, D.-Y., and Yoshida, K., "Transition Measurement System of Experimental Supersonic Transport NEXST-1, *Proceedings of International Congress of the Aeronautical Sciences, 2006-3.3.2* [CD-ROM], Optimage, Edinburgh, Sept. 2006.

[17] Kwak, D.-Y., Yoshida, K., Ishikawa, H., and Noguchi, M., "Flight Test Measurements of Surface Pressure on Unmanned Scaled Supersonic Experimental Airplane," AIAA Paper 2006-3483, June 2006.

[18] Kwak, D.-Y., Yoshida, K., and Noguchi, M., "Surface Pressure Measurement System for the Flight Test on Supersonic Experimental Airplane (NEXST-1)," *Proceedings of the 37th Japan Society for Aeronautical and Space Sciences Annual Meeting*, Japan Society for Aeronautical and Space Sciences, Tokyo, April 2006, pp. 175–178 (in Japanese).

[19] Owen, F. K., Horstman, C. C., Stainback, P. C., and Wagner, R. D., "Comparison of Wind Tunnel Transition and Freestream Disturbance Measurements," *AIAA Journal*, Vol. 13, No. 3, 1975, pp. 266–269.

[20] Nishioka, M., Iida, S., and Ichikawa, Y., "An Experimental Investigation of the Stability of Plane Poissuille Flow," *Journal of Fluid Mechanics*, Vol. 72, No. 4, 1975, pp. 731–751. doi:10.1017/S0022112075003254

[21] Kwak, D.-Y., Yoshida, K., Noguchi, M., and Ishikawa, H., "Boundary Layer Transition Measurement Using Preston Tube on NEXST-1 Flight Test," AIAA Paper 2007-4173, June 2007.

[22] Yoshida, K., Kwak, D.-Y., Tokugawa, N., and Makino, Y.,. "Supersonic Experimental Airplane (NEXST-1): Aerodynamics and Measurement System Design," *Proceedings of the 37th Japan Society for Aeronautical and Space Sciences Annual Meeting*, Japan Society for

Aeronautical and Space Sciences, Tokyo, April 2006, pp. 42–45 (in Japanese).

[23] Kwak, D.-Y., Tokugawa, N., and Yoshida, K., "Demonstration of Aerodynamic Design Technologies on Supersonic Experimental Airplane (NEXST-1) by Flight Test," *Proceedings of 2006 Korean Society for Aeronautical and Space Sciences: Japan Society for Aeronautical and Space Sciences Joint International Symposium on Aerospace Engineering*, Korean Society for Aeronautical and Space Sciences, Seoul, Nov. 2006, pp. 176–182.

[24] Ishikawa, H., Kwak, D.-Y., and Yoshida, K., "CFD Analysis on Flight Test Results of Supersonic Experimental Airplane NEXST-1," AIAA Paper 2007-3925, June 2007.

[25] Kawakami, H., Takatoya, T., and Ishikawa, H., "Static Aeroelastic Analysis of Supersonic Experimental Airplane NEXST-1 Flight Test," AIAA Paper 2007-4174, June 2007.

[26] Tokugawa, N., and Yoshida, K., "Transition Detection on Supersonic Natural Laminar Flow Wing in the Flight," AIAA Paper 2006-3165, June 2006.

[27] Ishikawa, H., Kwak, D.-Y., Yoshida, K., and Kawakami, H., "CFD Analysis on the Flight Test Data of Supersonic Experimental Airplane," *Proceedings of the 44th Aircraft Symposium* [CD-ROM], Japan Society for Aeronautical and Space Sciences, Tokyo, April 2006 (in Japanese).

[28] Yoshida, K., Ueda, Y., and Ishikawa, H., "Transition Analysis on the Flight Test Results of Supersonic Experimental Airplane Using an e^N Method," *Proceedings of the 44th Aircraft Symposium* [CD-ROM], Japan Society for Aeronautical and Space Sciences, Tokyo, April 2006 (in Japanese).

[29] Joslin, R. D., "Aircraft Laminar Flow Control," *Annual Review of Fluid Mechanics*, Vol. 30, Jan. 1998, pp. 1–20. doi:10.1146/annurev.fluid.30.1.1